Supporting Information Online for

Modeling Organic Aerosols in a Megacity: Comparison of Simple and Complex Representations of the Volatility Basis Set Approach

[1,*]Manish Shrivastava, [1]Jerome Fast, [1]Richard Easter, [1]William I. Gustafson Jr., [1]Rahul A. Zaveri, [2]Jose L. Jimenez, [3]Pablo Saide, and [4]Alma Hodzic

[1]Atmospheric Sciences & Global Change Division, Pacific Northwest National Laboratory, Richland, WA 99352

[2]University of Colorado, Boulder, CO

[3]Center for Global and Regional Environmental Research, University of Iowa, Iowa City, Iowa, USA

[4]National Center for Atmospheric Research, Boulder, CO

[*]Corresponding author: ManishKumar.Shrivastava@pnl.gov

The main text describes implementation of three WRF-Chem modeling cases evaluating OA formation against highly time resolved AMS PMF measurements using the MILAGRO 2006 case study in Mexico City. The supporting information presented here complements the main text providing further details including figures and discussions comparing the 9-species and 2-species VBS approaches at other ground sites and along aircraft flight transects.

S1.0. Evaluation of OA at remote sites

In the main text we evaluated OA predictions at two ground sites: an urban T0 site and suburban T1 site at the edge of the city. It is also instructive to evaluate OA variations at sites located farther from the city. In this section we look at two remote sites: T2 and Altzomoni. The T2 site was located 35 km to the north north-east of T1 at Rancho la Bisnaga, at an altitude of 2542 m. There are few significant anthropogenic emission sources between T1 and T2, and somewhat higher concentrations of OC and EC were found at T2 during periods of southwesterly winds (Doran, 2007). The mountain site of Altzomoni was located 60 km south-east of Mexico City at an altitude of 4010m (Baumgardner et al., 2009). The Altzomoni site is generally above regional mixed layer from late evening until late morning. The T2 and Altzomoni sites are indicated in Figure 1a.

Using a thermal-optical OC/EC analyzer, Doran et al. (2007) reported organic carbon (OC) concentrations at the T2 site, which are converted to OA using an OM/OC ratio of 1.4. Another way would be to derive OC from WRF-Chem predictions for direct comparison to measured OC. However, both methods have uncertainties associated with OM/OC ratio, as OC emissions in the inventory are derived assuming fixed OM/OC of 1.25 for fossil and 1.57 for biomass emissions. In addition, traditional biogenic and anthropogenic SOA in WRF-Chem need

to be converted to OC. In this work, we choose the former method of comparing OA instead of OC, acknowledging the inherent uncertainties with both approaches. Figure S1a and S1b compare 24-day average diurnal variations of OA and SOA from the 3 modeling cases. AMS OOA is not available for comparison to model predictions in Figure S1b. Figure S1a shows that Case 2 and Case 3 reasonably predict concentrations of OA. Also no strong diurnal variation in absolute OA concentrations at T2 site is apparent. A comparison of Figure S1a and S1b shows that model predictions indicate SOA to be dominant component of OA at this site throughout the day.

Figure S1c and S1d show 24-day average diurnal variations of OA and SOA respectively at the high altitude Altzomoni site. The top of the mixed layer reaches the altitude of Altzomoni at about 11-12 LT and remains above this altitude until after 20 LT. All modeling scenarios reproduce magnitude and diurnal variation of measured OA concentrations (using AMS) as shown in Figure S1c. As expected, both OA and SOA concentrations increase at this site after 11 LT as the top of the mixed layer reaches the altitude of 4 km. As with the T2 site, most of the simulated OA at the Altzomoni site is comprised of SOA.

S1.1. Evaluation of OA components aloft

AMS measurements aloft are available from G-1 (Kleinman et al., 2008) and C-130 (DeCarlo et al., 2008) aircraft flight transects. The two aircrafts made several transects on different days flying above the center of Mexico City and downwind. This data is valuable for studying time evolution and growth of organic aerosols due to gas-particle partitioning and photochemical aging of organics in the atmosphere. In this study, high time-resolution AMS PMF data (10-s data) from eight G-1 flights including 6a, 7a, 15a, 18a, 19a, 20a, 20b, 22a (a and b refer to morning and afternoon flights), and two C-130 flights (on March 10 and 29) are used

to evaluate simulated OA. The G-1 aircraft flew over Mexico City and up to 50 km northeast of the city, whereas the C-130 also flew farther downwind over the Gulf of Mexico.

Figure S2 compares WRF-Chem output for Case 2 vs. PMF results from the AMS aboard the G-1 and C-130 flights. Results are shown as scatter plots of mass concentrations vs. CO mixing ratios. Higher CO mixing ratios ($\geq$ 500 ppbv) are generally associated with the city center or within fire plumes, while lower CO mixing ratios represent instances when aircrafts were flying farther downwind. Figure S2a and S2c show that HOA is significantly under-predicted aloft over Mexico City and immediately downwind of city. HOA predictions improve at farther downwind locations (CO mixing ratios lower than 250 ppb). SOA predictions in Figures S2b and S2d show the reverse trend as compared to HOA. SOA predictions are much better over the city and immediate downwind locations, but SOA is over-predicted as compared to AMS OOA at more remote downwind locations. The two branches appearing in HOA and SOA scatter plots for Case 2 predictions in Figure S2 are interesting. In Figure S2b, the first branch showing high SOA at low CO concentrations (below 250 ppb CO) comes mainly from higher anthropogenic A-SI-SOA contributions for five G-1 flight paths. Higher BB-SI-SOA contributed to higher SOA at downwind locations for the remaining three G-1 flight paths on 15th, 18th and 19th March at downwind locations as compared to within the city. In Figure S2d, some of the highest SOA predictions at downwind locations are caused by high A-SI-SOA on 10th March 2006. High BB-SI-SOA also contributes to downwind SOA on both 10th and 29th March 2006. Significant contributions of A-SI-SOA downwind are also consistent with the high downwind HOA branch from model predictions appearing in both Figures S2a and S2c. In comparison to model predictions, PMF HOA shows more scatter (Figures S2a and S2c). The model has difficulty representing this scatter, thus highlighting significant uncertainties in representation of spatial

and temporal variation of emission sources in the 2006 MCMA inventory. This inconsistency related to uncertainties in emissions inventory has also been shown in previous work by Fast et al. (2009).

S2.0. Non-fossil carbon fraction (f_{NF})

^{14}C measurements provide insights into relative contributions of fossil and modern carbon. These measurements provide another metric to evaluate predictions of source-oriented models such as WRF-Chem. Substantial amounts of non-fossil carbon as a fraction of total OC (f_{NF}) are observed in both urban locations such as Mexico City and in remote environments of the Northern Hemisphere throughout the year (Hodzic A., 2010) . High values of f_{NF} observed in urban environments such as Mexico City during low biomass burning events points towards importance of representing non-fossil sources in emission inventories (Hodzic A., 2010). These sources include biogenic SOA, primary biological particles (PBAP) and urban sources of non-fossil carbon such as food cooking, municipal trash burning, biofuel use, etc.

In this work f_{NF} is calculated using following assumptions: 20% of urban carbon (both primary and secondary) is non-fossil, 15% of biogenic SOA is PBAP consistent with results from Hodzic et al. (2010), and both BBOA and SOA from biomass burning are non-fossil carbon sources. f_{NF} is not sensitive to dilution effects resulting from variation in boundary layer height as it is a ratio. Also f_{NF} does not depend on amount of oxygen added in the S/IVOC oxidation parameterization, as it is based on carbon fraction.

The non-fossil carbon fraction (f_{NF}) is found to range from 0.37-0.67 at T0 and 0.50-0.86 at T1, with a substantial disagreement between two datasets collected by two different groups, which remains unresolved (Hodzic A., 2010). Figure S3 shows the average diurnal variation of f_{NF} at the T0 and T1 sites respectively using Case 2 indicated by solid lines. The figure shows f_{NF}

values ranging from 0.26-0.40 and 0.34-0.43 at the T0 and T1 sites respectively. Consistent with estimations by Hodzic et al. (2010), f_{NF} values at the T1 site are predicted to be higher by about 0.1 as compared to the T0 site. Also, Figure S3 indicates that f_{NF} values at both sites increases during the day after 08 LT with a peak value at 18 LT.

We note that B-V-SOA is too low in our model compared to previous studies as discussed earlier. So, f_{NF} is recalculated in our model by increasing B-V-SOA by a factor of 5 at the T0 and T1 sites as indicated by dashed lines in Figure S3, keeping concentrations of all other OA components unaltered. Increasing B-V-SOA causes an increase in f_{NF} by 0.04 and 0.05 at the T0 and T1 sites respectively on an average.

It is also important to note that WRF-Chem predicts f_{NF} (average ~0.36 at T0 when biogenic SOA is corrected as above) which are slightly lower than the Aiken et al. (2010) f_{NF} dataset (average of 0.44), consistent with the results of Hodzic et al. (2010). Since WRF-Chem has missing biomass emissions especially during early morning which strongly affect the surface average concentrations (Aiken et al., 2010), increasing amount of biomass burning emissions would help to increase predicted values of f_{NF} bringing them into agreement to measurements, consistent with the conclusions of Hodzic et al. (2010). However a separate dataset of f_{NF} from Marley et al. (2009) reports f_{NF} which is larger by about 0.15 compared to the Aiken et al. (2010) data, and the unexplained disagreement between these datasets limits our ability to make strong conclusions based on these comparisons. In addition, accurate quantification of OA and S/IVOC emissions and their non-fossil carbon fraction for anthropogenic trash burning observed within and around Mexico City, as well as for other urban emissions such as food cooking and biofuel use is also essential to better constrain model predictions of f_{NF}.

S3.0. WRF-Chem vs. CHIMERE

Even though CHIMERE and WRF-Chem have differences in treatments of meteorology, chemistry, emissions, and coupling of meteorology with chemistry (offline versus online) they are widely used by different groups and it is instructive to compare OA predictions between the two models. WRF-Chem uses SAPRC-99 gas phase chemistry, whereas CHIMERE uses the MELCHIOR chemical mechanism. Details of the SOA formation mechanism in CHIMERE are discussed by Hodzic et al. (2009) and Hodzic et al. (2010). Since SI-SOA formation is primarily controlled by OH concentrations, inter-comparison of OH concentrations simulated by CHIMERE and WRF-Chem was done at the T0 site in Mexico City. Both models showed similar diurnal variations for OH, however, CHIMERE predicts higher average OH concentration as compared to WRF-Chem.

Also, in CHIMERE, dry deposition of all gaseous semi-volatile species is calculated similar to NO_2 (effective Henry's law constant of 0.01 M atm^{-1}), however, in WRF-Chem dry deposition is calculated using an effective Henry's law constant of 2700 M atm^{-1}. Hence dry deposition velocities of semi-volatile organic vapors in WRF-Chem are expected to be higher than CHIMERE. However, dry deposition velocities do not directly scale with effective Henry's law constant due to other factors as aerodynamic resistance, surface resistance, stomatal resistance and effect of reactivity on mesophyllic resistance (Bessagnet et al., 2010). Bessagnet et al. (2010) found that omitting dry deposition of semivolatile species may overestimate SOA concentrations by as much as 50% especially during nighttime when relative humidity is high. Quantifying effects of dry deposition on SOA concentrations is a subject for further study.

Figure S4 and S5 compare total OA, HOA, SOA and BBOA predictions at the T0 and T1 sites respectively from CHIMERE (using the ROB approach) and WRF-Chem (Case 2). Temporally averaged simulated values from both the models are also indicated on each figure.

The CHIMERE simulations of Hodzic et al. (2010) used an older POA emissions inventory for Mexico City, while the current WRF-Chem predictions are from a recently revised inventory for Mexico City for 2006, with an additional doubling of the default anthropogenic S/IVOC emissions (Case 2 Cases) used for comparison. Older POA emissions used by Hodzic et al. (2010) were greater than revised 2006 inventory used in this work by almost a factor of 2 at the T0 site, so Case 2 predictions of HOA are similar to Hodzic et al. (2010). At the T0 site, the average predictions of total OA, HOA, SOA and BBOA are very similar in both models. This is encouraging as it implies that simulated OA components by the two models within Mexico City are of similar order. Differences in temporal variations between WRF-Chem and CHIMERE are also due to different treatments of meteorology. WRF-Chem using online meteorology as discussed earlier which is more useful for simulating event periods, while CHIMERE uses offline meteorology through MM5.

At the T1 site, shown in Figure S5a, WRF-Chem predicts on average 25% higher total OA as compared to CHIMERE. Also, on an average WRF-Chem predicts lower HOA (10% lower) and higher SOA (50% higher) as compared to the CHIMERE model as shown in Figure S5b and S5c respectively. The S/IVOC emissions have had more time for multi-generational photochemistry leading to higher SOA/ΔCO ratios at the T1 site as compared to T0 site as discussed earlier. Differences in HOA are related to differences in emissions and spatial resolution of the model at the T1 site. As WRF-Chem assumes a minimum non-volatile fraction of 22% of SVOC emissions for anthropogenic emissions as compared to CHIMERE where the minimum non-volatile fraction is 9% (based on ROB approach), if emissions were same, WRF-Chem would predict higher HOA as compared to CHIMERE. In contrast, lower HOA predictions from WRF-Chem indicate significant differences in emissions, transport and

183 deposition between the two models. BBOA predictions are of the same order between
184 CHIMERE and WRF-Chem as shown in Figure S5d.

185 Figure S6 compares various SOA components between the two models at T1 site. Similar
186 amounts of traditional A-V-SOA are predicted by both WRF-Chem and CHIMERE as shown in
187 Figure S6a. CHIMERE predicts 5 times higher B-V-SOA as compared to WRF-Chem shown in
188 Figure S6b as discussed earlier. Figure S6c and S6d show that WRF-Chem predicts twice as
189 much A-SI-SOA and 50% higher BB-SI-SOA compared to CHIMERE, on average, with most of
190 the higher predictions occurring after March 24th. Differences in meteorological treatments
191 between the two models are partly responsible for differences in predicted OA. Higher SI-SOA
192 predictions from WRF-Chem are also partially caused due to the addition of 15% oxygen mass
193 per generation of oxidation as compared to 7.5% added oxygen assumed by CHIMERE model.
194 In addition, CHIMERE included treatment of precipitation and wet deposition (Hodzic et al.,
195 2010), which would have greatest impact after March 24, but the amount of aerosols removed by
196 wet deposition in CHIMERE was not quantified in that study. In contrast, wet deposition is
197 excluded in WRF-Chem in the present study, as Fast et al. (2009) found that effects of wet
198 deposition removal during that period was relatively small.
199
200
201
202
203
204
205

206 **S4.0. References**

207 Aiken, A. C., de Foy, B., Wiedinmyer, C., DeCarlo, P. F., Ulbrich, I. M., Wehrli, M. N., Szidat,
208 S., Prevot, A. S. H., Noda, J., Wacker, L., Volkamer, R., Fortner, E., Wang, J., Laskin, A.,
209 Shutthanandan, V., Zheng, J., Zhang, R., Paredes-Miranda, G., Arnott, W. P., Molina, L. T.,
210 Sosa, G., Querol, X., and Jimenez, J. L.: Mexico city aerosol analysis during MILAGRO using
211 high resolution aerosol mass spectrometry at the urban supersite (T0) - Part 2: Analysis of the
212 biomass burning contribution and the non-fossil carbon fraction, Atmos. Chem. Phys., 10, 5315-
213 5341, 10.5194/acp-10-5315-2010, 2010.
214 Baumgardner, D., Grutter, M., Allan, J., Ochoa, C., Rappenglueck, B., Russell, L. M., and
215 Arnott, P.: Physical and chemical properties of the regional mixed layer of Mexico's Megapolis,
216 Atmos. Chem. Phys., 9, 5711-5727, 2009.
217 Bessagnet, B., Seigneur, C., and Menut, L.: Impact of dry deposition of semi-volatile organic
218 compounds on secondary organic aerosols, Atmos. Environ., 44, 1781-1787,
219 10.1016/j.atmosenv.2010.01.027, 2010.
220 DeCarlo, P. F., Dunlea, E. J., Kimmel, J. R., Aiken, A. C., Sueper, D., Crounse, J., Wennberg, P.
221 O., Emmons, L., Shinozuka, Y., Clarke, A., Zhou, J., Tomlinson, J., Collins, D. R., Knapp, D.,
222 Weinheimer, A. J., Montzka, D. D., Campos, T., and Jimenez, J. L.: Fast airborne aerosol size
223 and chemistry measurements above Mexico City and Central Mexico during the MILAGRO
224 campaign, Atmos. Chem. Phys., 8, 4027-4048, 2008.
225 Doran, C.: "The T1-T2 study: evolution of aerosol properties downwind of Mexico City (vol 7,
226 pg 1585, 2007), Atmos. Chem. Phys., 7, 2197-2198, 2007.
227 Fast, J., Aiken, A. C., Allan, J., Alexander, L., Campos, T., Canagaratna, M. R., Chapman, E.,
228 DeCarlo, P. F., de Foy, B., Gaffney, J., de Gouw, J., Doran, J. C., Emmons, L., Hodzic, A.,
229 Herndon, S. C., Huey, G., Jayne, J. T., Jimenez, J. L., Kleinman, L., Kuster, W., Marley, N.,
230 Russell, L., Ochoa, C., Onasch, T. B., Pekour, M., Song, C., Ulbrich, I. M., Warneke, C., Welsh-
231 Bon, D., Wiedinmyer, C., Worsnop, D. R., Yu, X. Y., and Zaveri, R.: Evaluating simulated
232 primary anthropogenic and biomass burning organic aerosols during MILAGRO: implications
233 for assessing treatments of secondary organic aerosols, Atmos. Chem. Phys., 9, 6191-6215,
234 2009.
235 Hodzic, A., Jimenez, J. L., Madronich, S., Aiken, A. C., Bessagnet, B., Curci, G., Fast, J.,
236 Lamarque, J. F., Onasch, T. B., Roux, G., Schauer, J. J., Stone, E. A., and Ulbrich, I. M.:
237 Modeling organic aerosols during MILAGRO: importance of biogenic secondary organic
238 aerosols, Atmos. Chem. Phys., 9, 6949-6981, 2009.
239 Hodzic, A., Jimenez, J. L., Madronich, S., Canagaratna, M. R., DeCarlo, P. F., Kleinman, L., and
240 Fast, J.: Modeling organic aerosols in a megacity: potential contribution of semi-volatile and
241 intermediate volatility primary organic compounds to secondary organic aerosol formation,
242 Atmos. Chem. Phys., 10, 5491-5514, 10.5194/acp-10-5491-2010, 2010.
243 Hodzic A., J. J. L., Prevot A.S.H., Szidat S., Fast J.D., Madronich S.: Can 3-D models explain
244 the observed fractions of fossil and non-fossil carbon in and near Mexico City?, Atmospheric
245 Chemistry and Physics Discussions, 10, 14513-14556, 2010.
246 Kleinman, L. I., Springston, S. R., Daum, P. H., Lee, Y. N., Nunnermacker, L. J., Senum, G. I.,
247 Wang, J., Weinstein-Lloyd, J., Alexander, M. L., Hubbe, J., Ortega, J., Canagaratna, M. R., and
248 Jayne, J.: The time evolution of aerosol composition over the Mexico City plateau, Atmos.
249 Chem. Phys., 8, 1559-1575, 2008.

250 Kroll, J. H., Ng, N. L., Murphy, S. M., Flagan, R. C., and Seinfeld, J. H.: Secondary organic
251 aerosol formation from isoprene photooxidation, Environ. Sci. Technol., 40, 1869-1877,
252 10.1021/es0524301, 2006.
253 Marley, N. A., Gaffney, J. S., Tackett, M., Sturchio, N. C., Heraty, L., Martinez, N., Hardy, K.
254 D., Marchany-Rivera, A., Guilderson, T., MacMillan, A., and Steelman, K.: The impact of
255 biogenic carbon sources on aerosol absorption in Mexico City, Atmos. Chem. Phys., 9, 1537-
256 1549, 2009.
257 Ng, N. L., Chhabra, P. S., Chan, A. W. H., Surratt, J. D., Kroll, J. H., Kwan, A. J., McCabe, D.
258 C., Wennberg, P. O., Sorooshian, A., Murphy, S. M., Dalleska, N. F., Flagan, R. C., and
259 Seinfeld, J. H.: Effect of NOx level on secondary organic aerosol (SOA) formation from the
260 photooxidation of terpenes, Atmos. Chem. Phys., 7, 5159-5174, 2007a.
261 Ng, N. L., Kroll, J. H., Chan, A. W. H., Chhabra, P. S., Flagan, R. C., and Seinfeld, J. H.:
262 Secondary organic aerosol formation from m-xylene, toluene, and benzene, Atmos. Chem. Phys.,
263 7, 3909-3922, 2007b.
264 Tsimpidi, A. P., Karydis, V. A., Zavala, M., Lei, W., Molina, L., Ulbrich, I. M., Jimenez, J. L.,
265 and Pandis, S. N.: Evaluation of the volatility basis-set approach for the simulation of organic
266 aerosol formation in the Mexico City metropolitan area, Atmos. Chem. Phys., 10, 525-546, 2010.
267
268

269

270

271

Table S1. SOA mass yields using a 4-product VBS with C^* of 1, 10, 100 and 1000 μg m^{-3} for *V-SOA* precursors

V-SOA precursors	Aerosol Yield High NOx Parameterization				Aerosol Yield Low NOx parameterization			
	1	10	100	1000	1	10	100	1000
ALK4	N/A	0.038	N/A	N/A	N/A	0.075	N/A	N/A
ALK5	N/A	0.15	N/A	N/A	N/A	0.3	N/A	N/A
OLE1	0.001	0.005	0.038	0.15	0.005	0.009	0.06	0.225
OLE2	0.003	0.026	0.083	0.27	0.023	0.044	0.129	0.375
ARO1	0.01	0.24	0.45	0.7	0.01	0.24	0.7	0.7
ARO2	0.01	0.24	0.45	0.7	0.01	0.24	0.7	0.7
ISOP	0.001	0.023	0.015	0	0.009	0.03	0.015	0
TERP	0.012	0.122	0.201	0.5	0.107	0.092	0.359	0.6
SESQ	0.075	0.15	0.75	0.9	0.075	0.15	0.75	0.9

283

284

285 **Table S2.** V-SOA 1-product mass yields

V-SOA precursors	Aerosol Yield High NO_x (1 µg m^{-3})	Aerosol Yield Low NO_x (1 µg m^{-3})	Reference
ARO1	0.08	0.304	(Ng et al., 2007b)
ARO2	0.035	0.367	(Ng et al., 2007b)
TERP	0.066	0.379	(Ng et al., 2007a)
SESQ	0.847	0.417	(Ng et al., 2007a)
ISOPRENE	0.038	0.01	(Kroll et al., 2006)
ALK4	0.038	0.075	(Tsimpidi et al., 2010)
ALK5	0.15	0.3	(Tsimpidi et al., 2010)
OLE1	0.001	0.005	(Tsimpidi et al., 2010)
OLE2	0.003	0.023	(Tsimpidi et al., 2010)

286

287

288

289

290

291

292

293

294

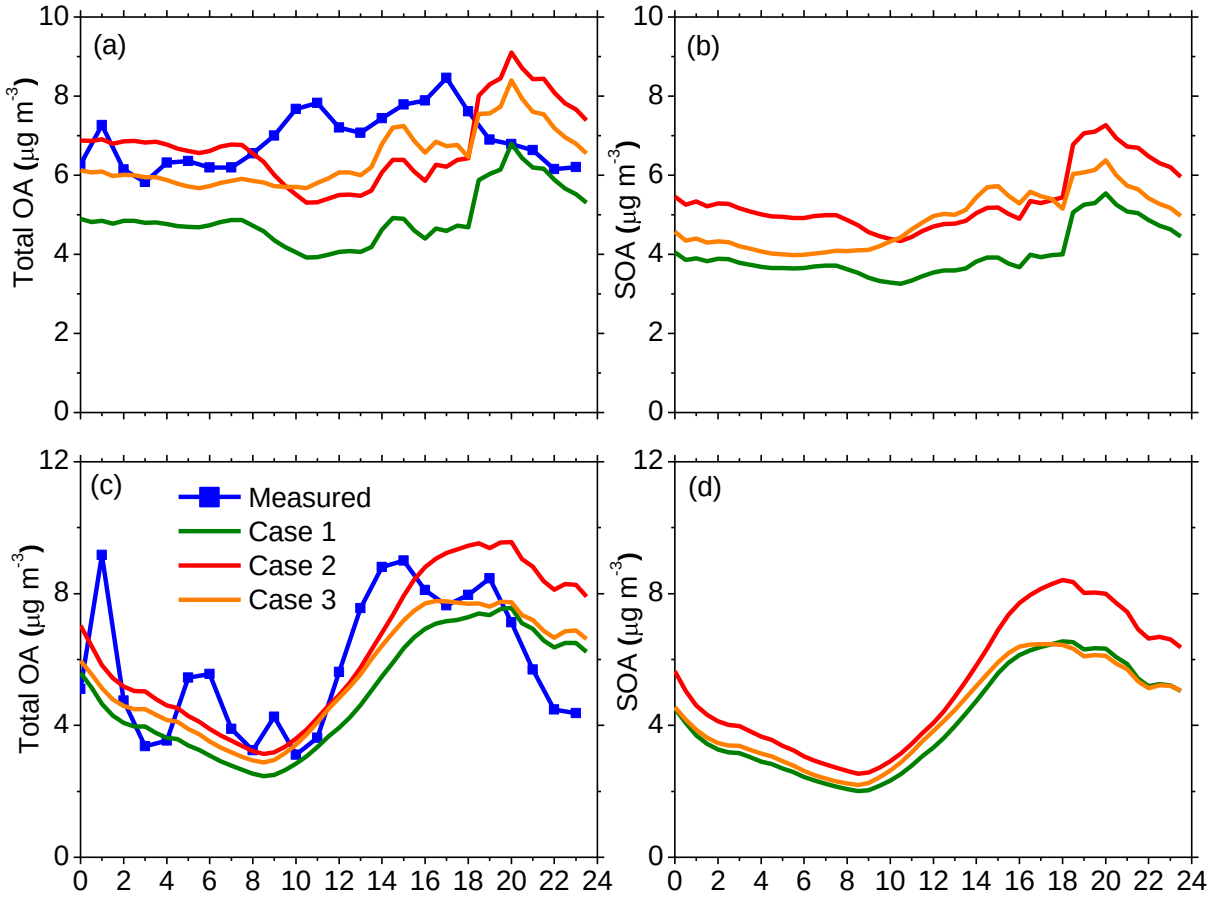

Figure S1: Average diurnal observed and simulated concentrations of (a) Total OA at T2 site (b) SOA at T2 site (c) Total OA at Altzomoni mountain site (d) SOA at Altzomoni mountain site. Location of T2 and Altzomoni sites are indicated in Figure 1a in the main text.

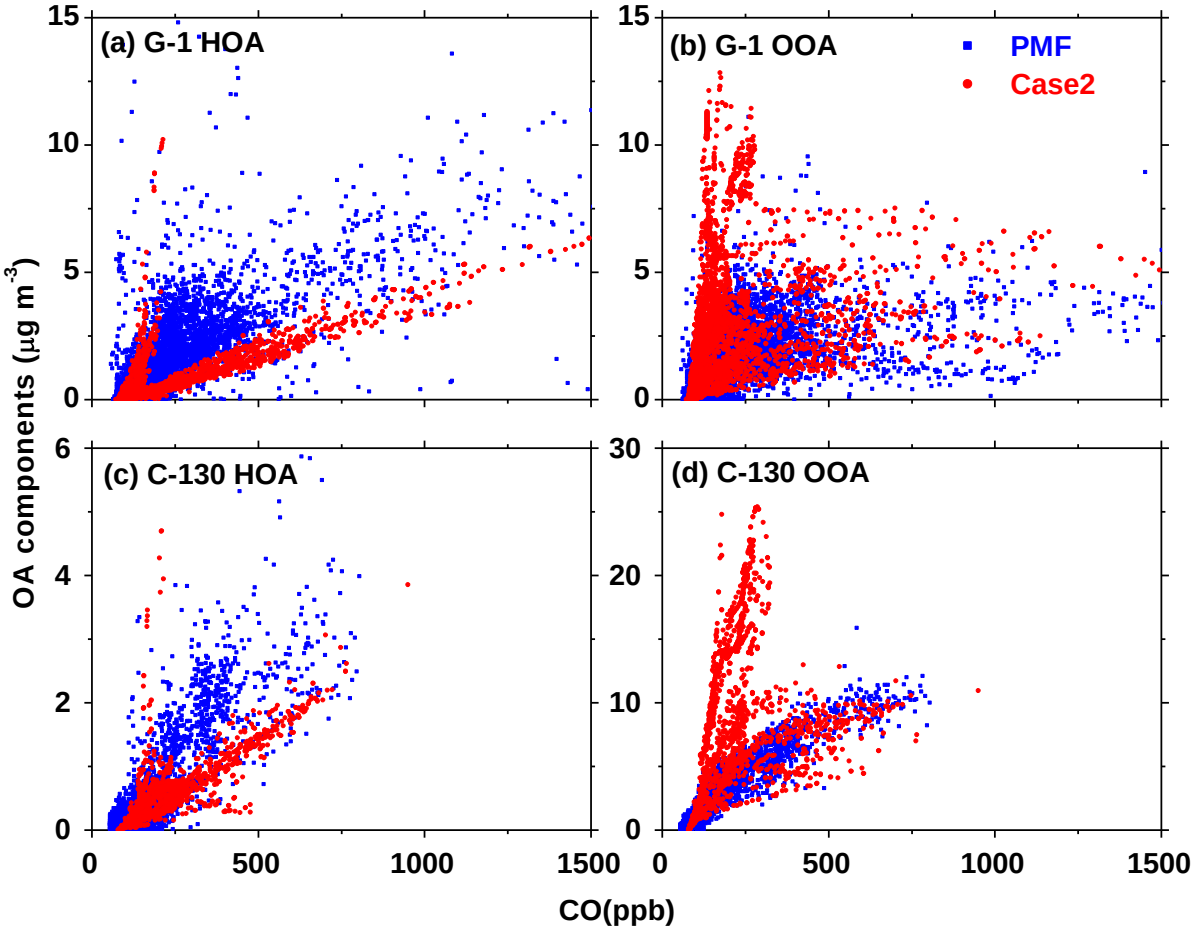

Figure S2: WRF-Chem (Case 2) predictions of OA components vs. CO mixing ratios (a) HOA for 8 G1 flights (b) OOA for 8 G-1 flights (c) HOA for 2 C-130 flights (d) OOA for 2 C130 flights

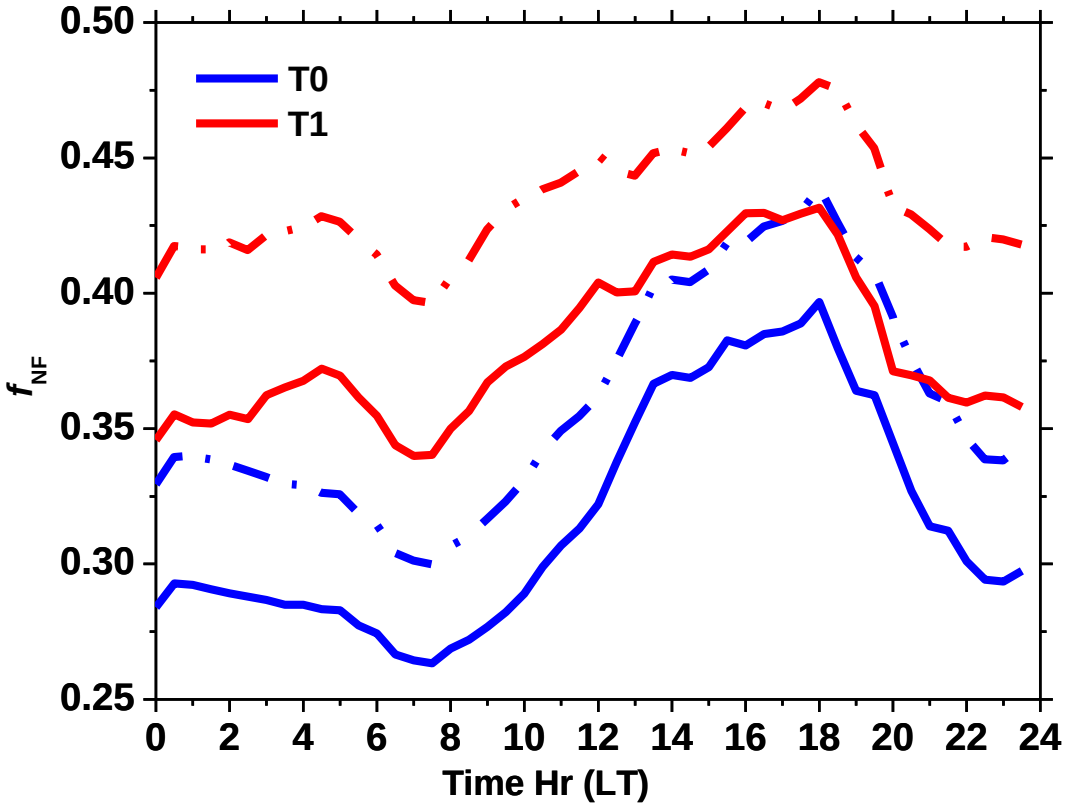

Figure S3: Average diurnal variation of non-fossil carbon fraction (f_{NF}) at the T0 and T1 sites in Mexico City region for March 6-30 2006. Solid lines represent Case 2 in this study, while dashed lines represent the same modeling Case (Case 2) with 5 times predicted biogenic B-V-SOA concentrations at T0 and T1 sites. Increasing biogenic SOA concentration by a factor of 5 increases predicted f_{NF} by 0.05 at both sites.

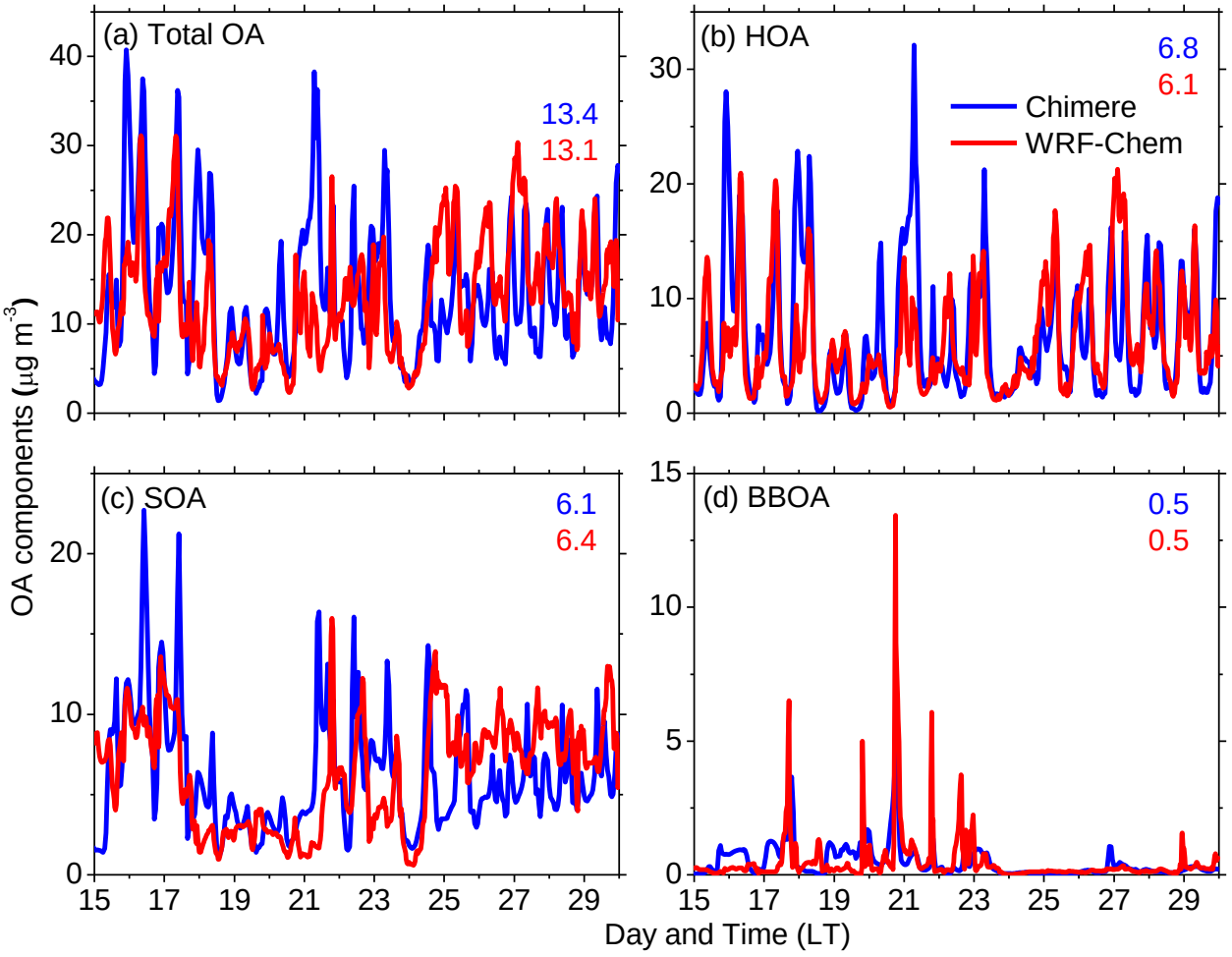

Figure S4: Comparing predictions of (a) total OA, (b) HOA, (c) SOA and (d) BBOA from CHIMERE (using the ROB approach) vs. WRF-Chem model (Case 2) at the T0 site in Mexico City. The mean predicted values from the two models are also indicated.

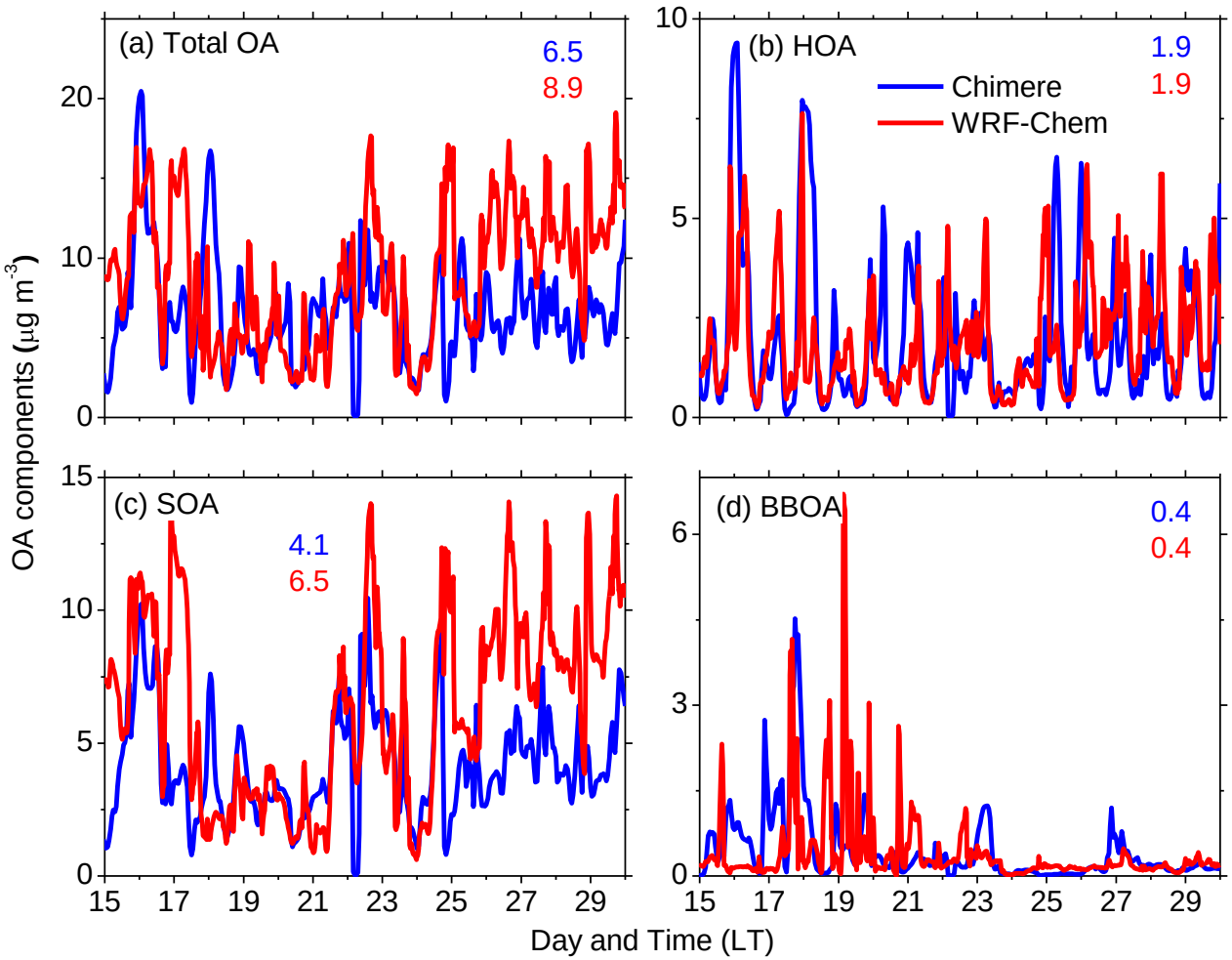

Figure S5: Comparing predictions of (a) total OA, (b) HOA, (c) SOA and (d) BBOA from CHIMERE (using the ROB approach) vs. WRF-Chem model (Case 2) at the T1 site in Mexico City. The mean predicted values from the two models are also indicated.

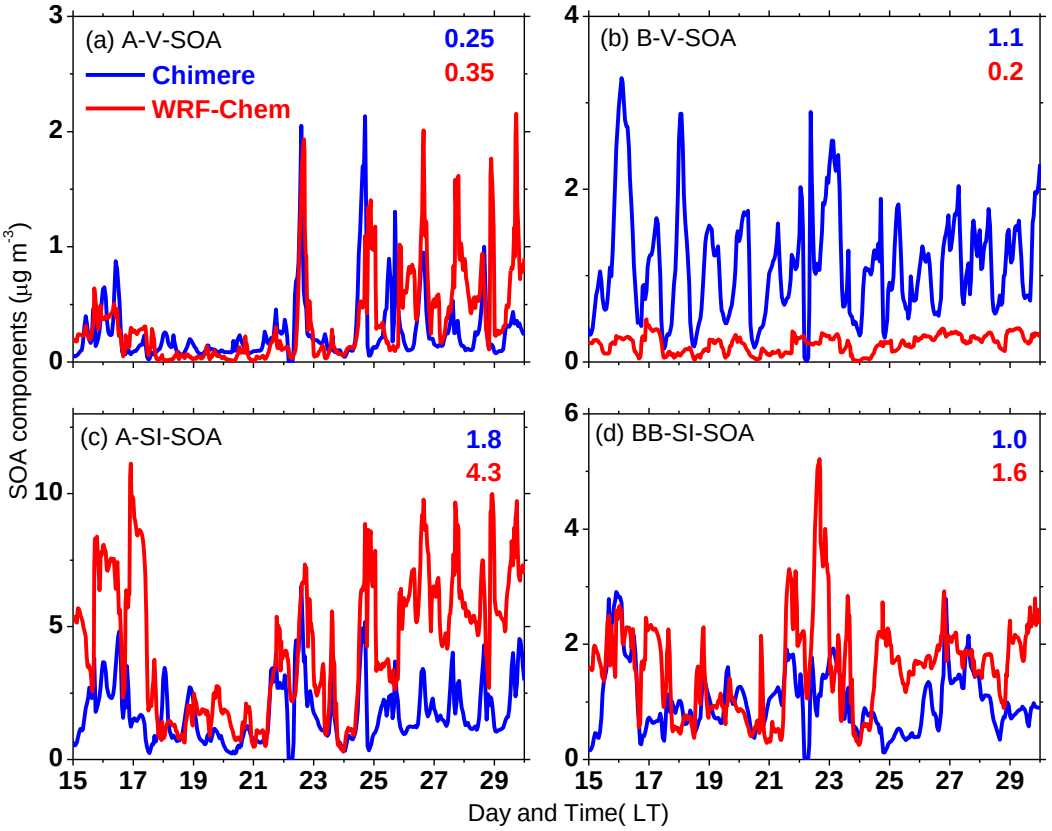

Figure S6: Comparing predictions of SOA components from CHIMERE (using the ROB approach) vs. WRF-Chem model at the T1 site in Mexico City (a) traditional ant V-SOA (b) biogenic V-SOA (c) anthropogenic SI-SOA (d) biomass burning SI-SOA. Temporally averaged values are also indicated on each figure.

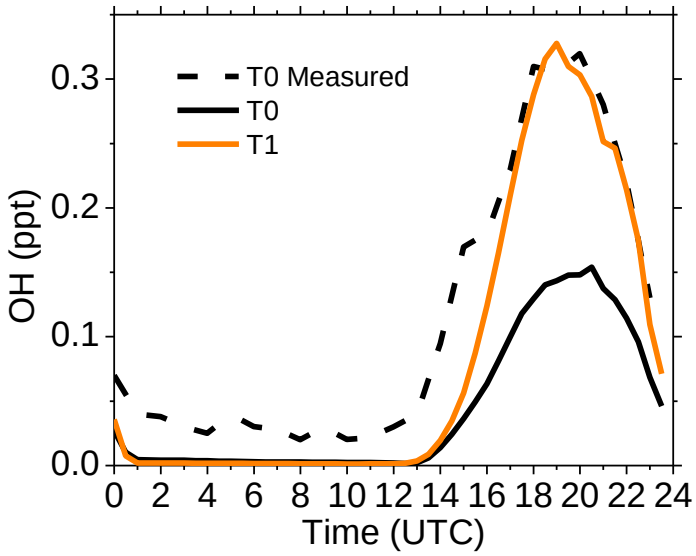

401

402 Figure S7: Comparison of measured vs. WRF-Chem predicted 24-day average diurnal variation
403 of OH concentration at T0 site in Mexico City. Predicted diurnal variation of OH at T1 site is
404 also included for comparison.